REVIEW OF SCIENTIFIC INSTRUMENTS **86**, 023708 (2015)

A novel technique for investigation of complete and partial anisotropic wetting on structured surface by X-ray microtomography

M. Santini,[1,a)] M. Guilizzoni,[2] S. Fest-Santini,[3] and M. Lorenzi[4]
[1]*Department of Engineering and Applied Sciences, University of Bergamo, Bergamo, Italy*
[2]*Department of Energy, Politecnico di Milano, Milano, Italy*
[3]*Department of Engineering, University of Bergamo, Bergamo, Italy*
[4]*School of Engineering and Mathematical Sciences, City University London, London, United Kingdom*

(Received 18 November 2014; accepted 3 February 2015; published online 19 February 2015)

An experimental study about the anisotropic wetting behavior of a surface patterned with parallel grooves is presented as an application example of a novel technique for investigation of complete and partial anisotropic wetting on structured surface by X-ray microtomography. Shape of glycerin droplets on such surface is investigated by X-ray micro computed tomography (microCT) acting as a non-intrusive, full volume 3D microscope with micrometric spatial resolution. The reconstructed drop volumes enable to estimate the exact volumes of the drops, their base contours, and 3D static contact angles, based on true cross-sections of the drop-surface couple. Droplet base contours are compared to approximate geometrical contour shapes proposed in the literature. Contact angles along slices parallel and perpendicular to the grooves direction are compared with each other. The effect of the sessile drop volume on the wetting behavior is discussed. The proposed technique, which is applicable for any structured surface, enables the direct measure of Wenzel ratio based on the microCT scan in the wetted region usually inapproachable by any others. Comparisons with simplified models are presented and congruence of results with respect to the minimum resolution needed is evaluated and commented. © *2015 AIP Publishing LLC.* [http://dx.doi.org/10.1063/1.4908171]

I. INTRODUCTION

Wetting phenomena on structured solid surface have received continued attention, driven by the potential applications of engineered surfaces with a well-defined chemical and/or topographical pattern in all the fields where wettability is an important design parameter.[1,2] The three-phase contact line of a droplet on ideal solid surfaces is represented by a circle, and the contact angle can be predicted by the well-known Young equation. However, real surfaces are, in general, heterogeneous and rough, and the drop and the three-phase contact line are distorted under the influence of the surface pattern and composition.[3] If the roughness geometry is isotropic, then the apparent contact-angle may be modeled by the Cassie-Baxter[4] and by the Wenzel[5] formulas for composite and homogeneous wetting, respectively. On the contrary, for anisotropic roughness, the apparent contact angle is no longer "uniform" along the three-phase contact line. A classical example (suitable as test case for the proposed novel technique) is the topography of surfaces with straight microfins, where a bi-dimensional profile is extruded along the third dimension. On such microfin surfaces, the drop is elongated in the direction parallel to the grooves and larger values of the cross-groove apparent contact angle are reported, when the three-phase contact line is parallel to the grooves.[6] This observation was attributed by the authors to the pinning of the droplet on the edges of the surface. Long *et al.*[7] have found that the apparent contact angle parallel to the groove is in a metastable state, whereby the equilibrium state depends on the number of grooves on which the drop resided.[6] Consequently, the volume of the drop is essentially influencing its base contour shape on grooved surfaces,[8] especially, for wetting drops in the same order of magnitude as the groove length scale.

The efforts to experimentally visualize the resulting drop-surfaces interface have been, up to now, limited to non-intrusive methods (as they should not alter the system dynamics and the fluid equilibrium), usually derived from optical applications.[9] In these cases, the focal path-length, the magnification, and the medium opaque to visible wavelength emerge as major limitations, in addition to the fact that bi-dimensional images only are acquired, which may misrepresent the local information. The presence of multiple grooves can lead to significantly scattered data close to the contact line due to the prevalence of hysteresis on patterned surface,[10] and their projection on a bi-dimensional image yields in an unfocused region in the view parallel to the grooves.

In this paper, the use of X-ray micro computed tomography (microCT), acting as a non-intrusive full volume 3D microscope with micrometric spatial resolution, is proposed to investigate the three-phase contact line of sessile drops on a grooved surface. The primary objective of this work is to visualize three-dimensionally the drop shape caused by the anisotropic surface topography. The acquisition of a three-dimensional representation of the drop and the substrate enables to understand the general qualitative feature of the three-phase contact line and to determine the real and apparent contact angles in any viewing direction. Furthermore, the use of microCT data to determine the real roughness ratio in the

[a)]Author to whom correspondence should be addressed. Electronic mail: maurizio.santini@unibg.it

TABLE I. Drop characteristics.

Drop	Voxel [μm]	V [mm^3]	r [μm]	Bo [-]	Covered ridges [-]
1	4.0	0.757 (±64 μm^3)	566 ± 4.0	0.062	4
2	4.0	3.638 (±64 μm^3)	954 ± 4.0	0.177	6
3	4.0	4.185 (±64 μm^3)	1000 ± 4.0	0.195	6
4	9.22	26.675 (±783.78 μm^3)	1854 ± 9.2	0.670	12
5	4.0	3.873 (±64 μm^3)	974 ± 4.0	0.185	7

Wenzel and in the Cassie-Baxter wetting regime is introduced and discussed.

II. MATERIALS AND METHODS

A. Setup and acquisition

At the University of Bergamo, a prototype microCT facility has been developed that consists of a microfocus X-ray cone-beam source, an air bearing rotation stage, and a CMOS flat panel detector. Magnification factor is in the range of 30 times, tube current and voltage are in the range of 100 μA and 50 kV, respectively. The isotropic voxel size, here, is 4 μm or 9.22 μm (Table I). Further details about the rig and a summary of the basic theory involved in the tomographic procedure can be found in Ref. 11, which also describes the validation of the technique for the extraction and estimation of the three-phase contact line on smooth surfaces. X-ray microCT was also used for wetting analysis of complex structured surfaces in Ref. 12. The X-ray images of drops and anisotropic patterned surface were acquired, and tomographic reconstructions were performed using standard filtered back-projection based on Feldkamp algorithm to obtain drop and surface volume, respectively.

B. Drop characteristics

Glycerol was selected for the experiments as a compromise is needed between a non-evaporating and a heavy fluid, which is more prone to gravitational sagging. For a drop with a radius of 1 mm, the evaporation effect on the drop dimensions during the acquisition was estimated to be less than 0.1 μm/h, a value which is lower than the overall scanning resolution.

By denoting ρ and σ as the density and surface tension of glycerol at 20 °C and r as the drop radius, the Bond (or Eötvös) number is Bo = $\rho gr^2/\sigma$, and its values for the studied droplets are summarized in Table I, showing that gravity influence on the analysed droplets profile is negligible. The drop radius is calculated from the microCT drop volume assuming an equivalent spherical shape, as commonly done in the literature. Figure 1 illustrates the variation of drop volumes and the ridges and grooves covered by the fluid between the two extreme drops investigated in this study.

To ensure that sessile drops in steady-state conditions are acquired, drops were placed gently on the sample, and the acquisitions were started after 12 h, thus guaranteeing that the drop had reached the equilibrium condition.

C. Surface characteristics

It was not the aim of the work to fabricate a micro-grooved surface, thus a vinyl music record is used as a suitable sample, following an idea reported in Ref. 13.[24] Its geometrical dimensions are extracted from the microCT reconstruction of the disc volume, see Figure 2, and are listed in Table II.

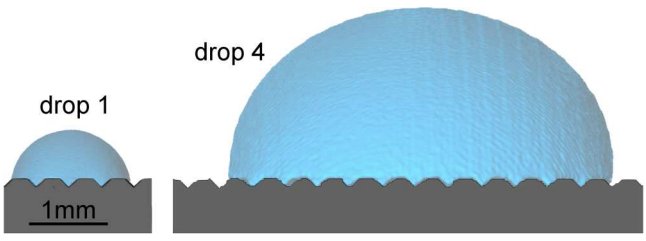

FIG. 1. Scaled comparison of rendered microCT drops, evidencing the volume variation and the different number of covered ridges and grooves between the smallest and the largest one.

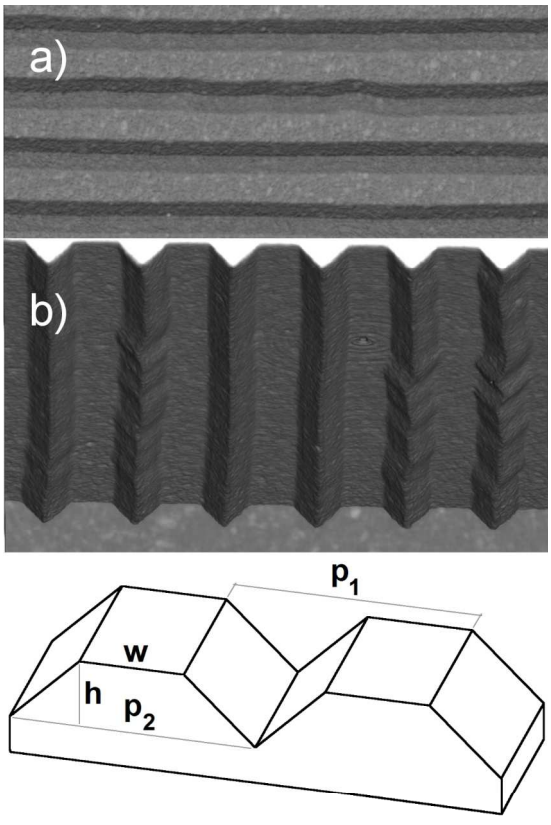

FIG. 2. The grooved surface as extracted by segmentation of volume rendered microCT: (a) Top view; (b) tilted side view, and its schematic outline.

TABLE II. Geometry of the grooved surface.

		[μm]
Groove height	h	92
Ridge width	w	136
Top pitch	p_1	320
Bottom pitch	p_2	320

D. Wetting analysis

The wetting behavior was analyzed in terms of drop shape, wetting state, real and apparent wetted area and Wenzel ratio, and real and apparent contact angles. All the investigated parameters were extracted from microCT reconstructions. The drop and the vinyl volumes were extracted by means of volume segmentation on the basis of the different X-ray attenuation. The base of the drop volume is the real wetted area, while its projection onto a horizontal plane gives the apparent wetted area. The analysis of the drop and surface contact area gives the information about the wetting state. Thus, it is possible to measure the roughness ratio of the wetted area, also called wetted area ratio, defined as the ratio between real microscopic wetted area and its projection on the reference plane. Here, such ratio is denoted with R_W for complete wetting and with R_{CB} for partial wetting. Similarly to what was done in Ref. 11, contact angle measurements were performed using a modified version—implemented in a home-made software—of the axisymmetric drop shape analysis (ADSA).[14] With respect to the commonly used ADSA, the use of microCT enables replacing the drop/surface side pictures with real slices of the drop and vinyl volumes in the chosen direction and at the chosen location. Thus, local information about both the real and the apparent contact angle along the triple line can be obtained, overcoming the limitation of the conventional optical approach based on side projections. Another difference, more specific for this case, is that the drop is very elongated so the assumption of axisymmetry on which the conventional ADSA is based is not correct. Therefore, the experimental drop contours were fitted with the numerical integration of the Laplace-Young equation written for a cylindrical drop. Such approximation to a "2D-extruded" shape, which again allows contact angle measurement by granting that each slice contains the normal to the liquid-vapor interface, is fairly good for the central part of the drop along the direction of the grooves, while in the border regions and in the cross-groove direction, it is quite coarse. A more rigorous approach would have been to calculate the normals to the reconstructed drop surface (e.g., approximating it as a triangle mesh) and then to slice the tomographic volume along a number of planes containing such normals. This would have been absolutely possible on the microCT reconstruction, but it would have implied losing the direct association of the estimated contact angle with the groove direction (grouping the results in terms of "parallel-to-the-grooves" and "perpendicular-to-the-grooves" directions), which is the main characteristic of the investigated surfaces. So, the cylindrical approximation was preferred.

The validation of the measurement technique was carried out (for axisymmetric drops) in previous works:[11] for images having the same quality level of the present microCT slices, the mean absolute error (MAE) is around 0.8° for drop with contact angles lower than 160°.

III. RESULTS AND DISCUSSION

A. Triple line analysis

Figures 3(a)–3(c) show the classical views of conventional bi-dimensional images of a segmented and rendered microCT drop (drop 1 of Table I): side, front, and top view, respectively. These views show a typical final shape of a wetting drop gently deposited onto the microfin, corrugated surface. Since the surface pattern is bi-dimensionally extruded, the advancing contact line behaves differently along the directions parallel and perpendicular to the grooves. Whereas on the one hand, no hysteresis due to surface patterning is expected in the parallel direction,[15] on the other hand, in the direction perpendicular to the grooves, surface grooves are known to pin the contact line.[16,17] This pinning leads to strong contact angle hysteresis and causes differences in the corresponding apparent contact angles as it will be discussed later on.

The top view, Figure 3(c), illustrates how the liquid spreads inside the grooves and fingers in extended liquid filaments for which the grooves act as confining compartments. These filaments can grow and shrink in length while the liquid cross section remains essentially constant.[18] If the volume of the drop is large enough, the liquid spills over the ridge edges and spreads into the neighboring grooves. Furthermore, the

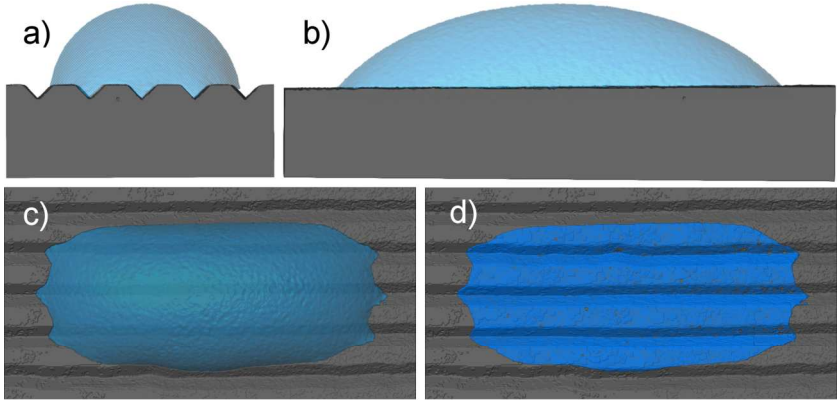

FIG. 3. Equilibrium shape of the microCT drop 1: (a) side view; (b) front view; (c) top view; and (d) corresponding contact surface.

liquid/vapor interface is curved toward the vapor and should be characterized by a positive Laplace pressure. According to Ref. 18, filaments could feature positive or negative pressure, and in the latter case, the interface would be curved toward the liquid.

Figure 3(d) shows the contact surface wetted by the fluid. It is worth emphasizing that the top view contour does not represent also the droplet base contour; this becomes especially true for drops on hydrophobic and superhydrophobic surfaces.

From the contact surface, the three-dimensional triple line is extracted, and its values are shown in Figure 4 both in Cartesian coordinates and projected in polar coordinates as a function of the azimuthal angle. It is already rather clear that the commonly used fits[6]—cubic or elliptical—based on the maximum spread extension in the side and front view, respectively, cannot describe the real triple line within the grooves.

In Figure 5, the extracted triple lines of all analyzed drops are confronted. For this purpose, their values are normalized by the drop equivalent radius.

For drops 1 to 3, for which the drop dimensions are comparable to the dimension of the grooves, a clear trend is visible. The larger is the relative ratio between the dimension of the drop and the dimension of the barriers, the larger is the drop elongation-ratio of the maximum base dimensions in parallel and perpendicular groove direction. This immediately implies that the difference between the drop contact angle perpendicular and parallel to the grooves is increased (compare Figure 9), a behavior that is confirmed by Ref. 6. The authors stated that fixed all the other parameters, the drop becomes longer as the number of contact ridges increases.

Further, the apparent contact angles in the front view are reduced. Again, none of the projected triple lines could be described by simple geometrical profiles.

Conversely, Figure 6(a) shows a slice of the drop volume (drop 2) at a height immediately above the contact region, where therefore the drop shape is influenced by the elongation caused by the surface topography but not directly affected by the groove presence. It could represent a top view of a non-wetting drop in case of a conventional bi-dimensional photo

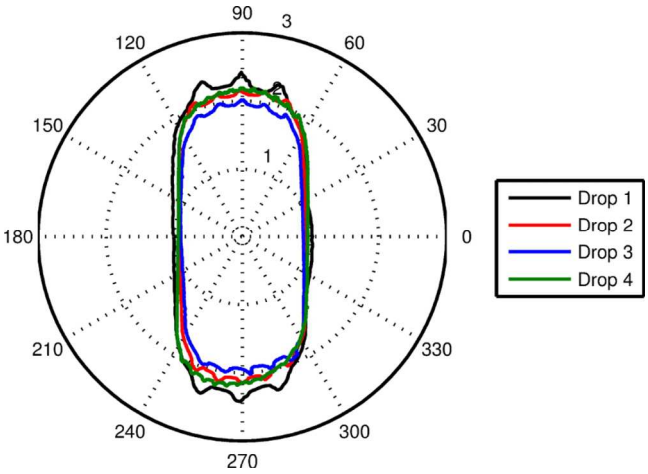

FIG. 5. Comparison between the normalized triple lines as a function of the azimuthal angle.

image. The contour of the slice is extracted (Figure 6(b)) and compared to geometrical base contour shapes representing the equivalent contact line in Figure 6(c). As stated in the literature,[6,19] in this case, cubic equations lead to a quite satisfactory agreement.

B. Wetting and contact line analysis

Drops 2 and 3 (compare Table I) offer rather similar volume and cover the same number of ridges, but their drop equilibrium shape and consequently drop base contour differ slightly.

For visualization propose, the volumes are superimposed in Figure 7, which may let conclude that different equilibrium drop shapes are possible for a similar liquid volume due to the deposition dynamics, allowing the technique to be used for investigating comparative scenarios.

For the investigated drops from 1 to 4, the wetting state is of the Wenzel type: the groove shape and dimensions let the liquid completely fill the grooves. Figures 8(a)–8(d) show some tomographic slices (from drop 2) perpendicular to the grooves, produced by moving the sectional plane from the

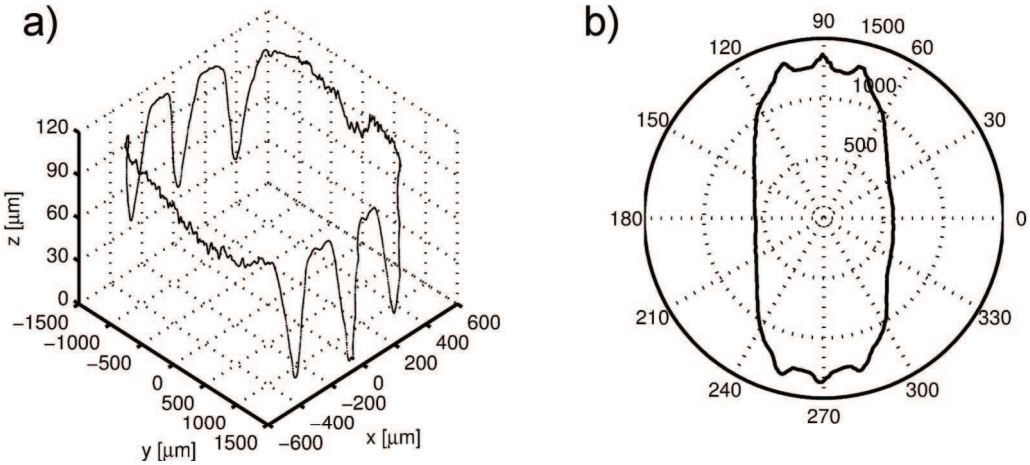

FIG. 4. 3D triple line in Cartesian coordinates (a). Projected triple line [μm] as a function of the azimuthal angle, (b). The Cartesian graph axes are not equally scaled to highlight the triple line details within the grooves.

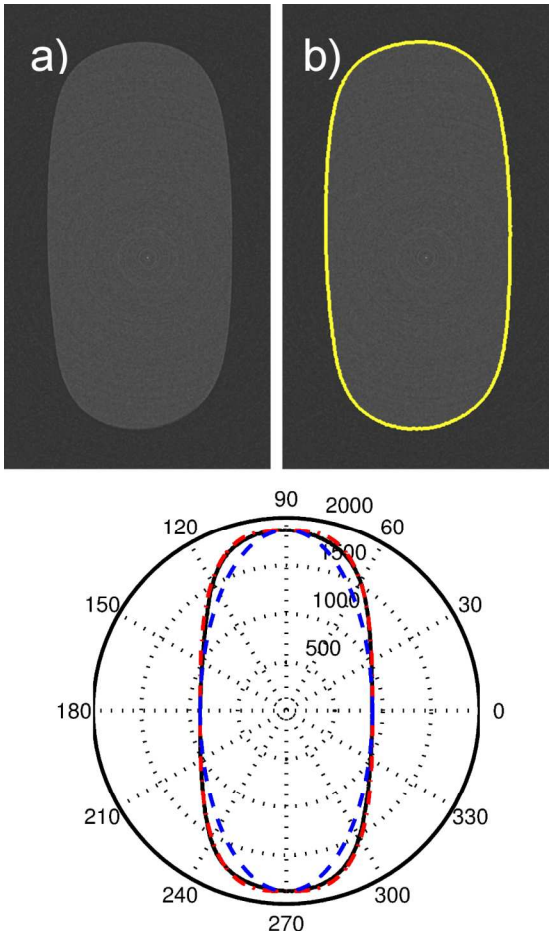

FIG. 6. Contour fitting based on microCT of drop 2: (a) slice at a height immediately above the contact region; (b) drop contour highlighted in yellow; and (c) comparison of extracted contour (black) with elliptic (dashed blue line) and cubic (dashed dotted red line) fits[6] as a function of the azimuthal angle (contour dimensions are in μm).

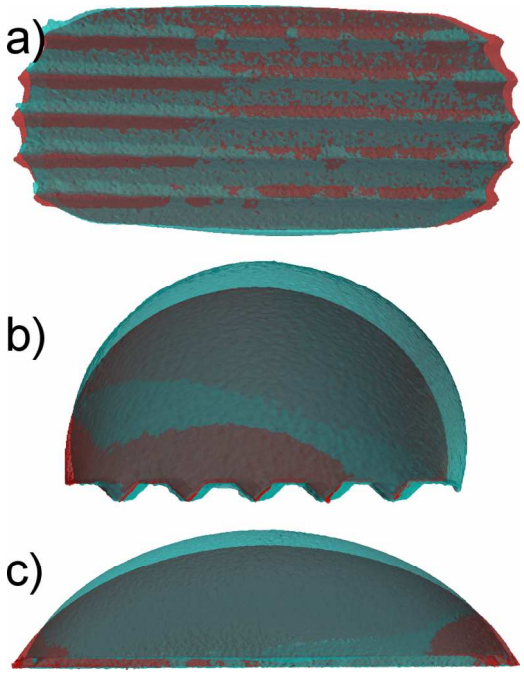

FIG. 7. Superposition of microCT drops 2 (red) and 3 (blue): (a) top view; (b) front view; and (c) side view.

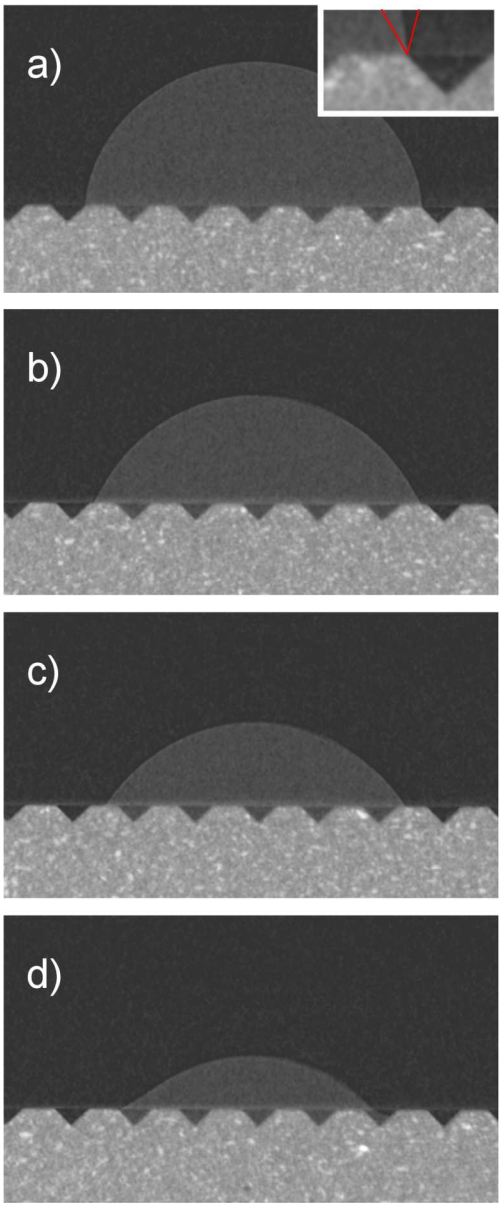

FIG. 8. Tomographic slices perpendicular to the grooves showing the change from advancing to receding contact lines at different cross-sections. Red lines evidence the contact angle limits according to Gibbs criterion.[20]

drop apex towards the end of the drop major axis. This image sequence, extracted for drop 2 but representative of the behavior of all drops 1–4, could be interpreted as the visualization of a change from advancing to receding contact line. In Figure 8(a), the liquid spreading over the ridges (after deposition and reaching of the equilibrium shape) has stopped at the outer ridge edge and could not over spill it, so that the triple line is pinned to the outer ridge edge. In this case, the apparent contact angle is 89.5°, and it can be seen as an advancing one. Finally, in Figure 8(d), the drop liquid is pinned to the inner ridge edge. Here, the liquid could not go beyond the edge and it spreads within the grooves forming extended filaments. The apparent contact angle versus the horizontal ridge plane is about 32° and it can be interpreted as a receding contact angle. On the contrary, the filament contact angle versus the groove sidewalls shows a much larger value, slightly larger than 60°,

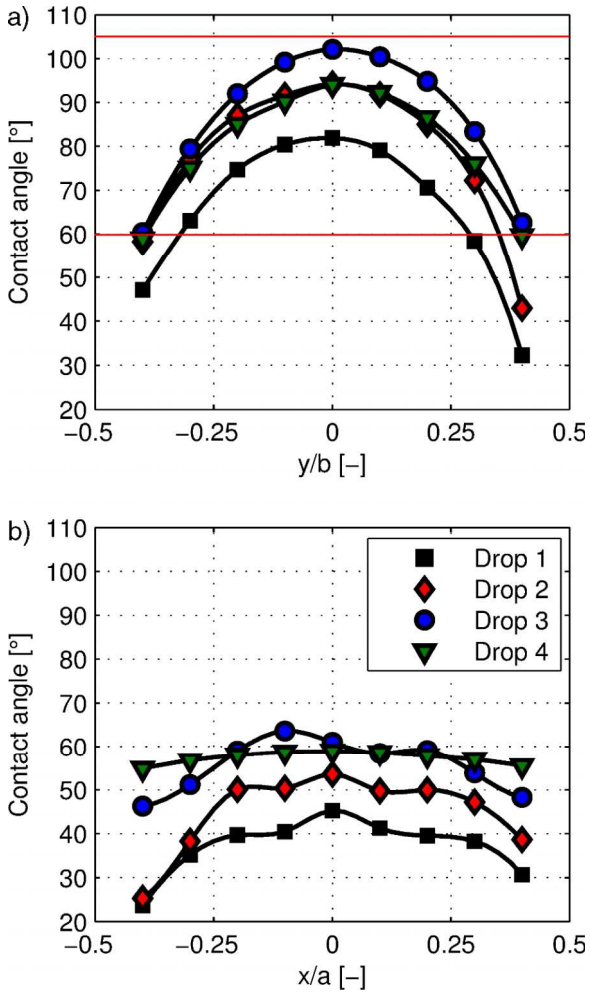

FIG. 9. Apparent contact angles measured along slices at different dimensionless distances from the drop apex: (a) perpendicular (red lines represent contact angle limits according to Gibbs criterion); (b) parallel to the grooves.

that is, the real contact angle value which could be measured both on the top of the ridges (Figures 8(b) and 8(c)) and on flat, smooth vinyl surfaces.

Figure 9 shows the results for measurements along slices perpendicular and parallel to the grooves, at different distances from the drop apex. To make the results for the investigated drops directly comparable, the slice distance from the drop apex was normalized with respect to the drop minor axis a for the slices parallel to the grooves, and with respect to the drop major axis b for the slices perpendicular to the grooves.

It is evident that for both directions, there is an evolution of the apparent contact angle along the drop diameters, showing a good symmetry with respect to the vertical planes passing through the drop apex. The only exception is the case of drop 4 in the direction parallel to the grooves, where the variation is very slight. It has to be noted that in the along-grooves direction, the surface sample is minimally inclined (about 0.5°) and this affected negatively the accuracy of contact angle measurements.

Such an inclination may also be one of the causes of the asymmetry of the measured contact angles in the along-grooves direction. Further causes of the asymmetry, particularly affecting on the contrary the values in the cross-grooves direction, may be searched in the deposition history and in metastable equilibria reached by the drop and in the already cited "cylindrical drop" approximation, which may result in a not accurate contact angle estimation in the most indented parts of the drop contour. These hypotheses are supported also by the fact that the asymmetry is larger for the two smaller drops.

The apparent contact angles on cross-groove planes are much larger, both of the angles in the along-grooves planes and of the static contact angle measured on flat surface, up to the point that they reach the limit of apparent hydrophobicity. This is due to the pinning of the triple line on the ridge edges. Such effect seems to be volume-dependent, but for the investigated drops, no univocal behavior could be identified as drops 2 and 3—which have similar volumes—show different results, and drop 4 inverts the trend traced by the other drops. This seems to support the already stated hypothesis that the results are also dependent on the deposition (influencing the drop configuration and the number of covered ridges), so that multiple drops of the same volume should be deposited to get more reliable information.

According to Gibbs theory,[20,21] the contact angle range due to pinning on groove edges should span from 60° (value for the smooth surface) to 105° (previous value plus inclination of the groove side walls). As it is reported in Figure 9(a), this is in very good agreement with the experimental results for the largest drops, while for the small ones the minimum measured contact angles are under the predicted lower bound. This may be due to the already cited extended filaments or due to the inaccuracies in the measurement, including the cylindrical drop approximation, which once again affects more heavily the smaller drops.

C. Real wetted area ratio

The calculation of the real wetted area ratio (R_W or R_{CW}) is still a very challenging problem with the traditional techniques, but using the microCT becomes possible to visualize, extract, and measure the real wetted surface (in Wenzel or Cassie-Baxter regimes or any transition between them) with micrometric resolution, together with its apparent projection on the reference plane.

Figure 10 shows for drops 1 to 4 that completely wet the vinyl surface, the real wetted contact area, and the corresponding apparent one. The latter is obtained as the area cut by the projection of the previously determined 3D triple line onto the reference plane.

In the case of complete wetting, the ratio R_W for an idealization of the investigated surface can be calculated by basic geometry using the values summarized in Table II for the geometrical features of the cross-section and considering it as extruded in the third dimension (neglecting the real shape of the triple line and the border effects near the latter).

Such an approach is obviously rather simplified but it offers an interesting opportunity of comparison with the values obtained by real 3D microCT scans.

From the latter, the calculation of the wetted area ratio presents its major point of difficulty in the measurement of the contact surface area. In fact, the latter is jagged, due to the digital, voxelized nature of the acquired volume. The same

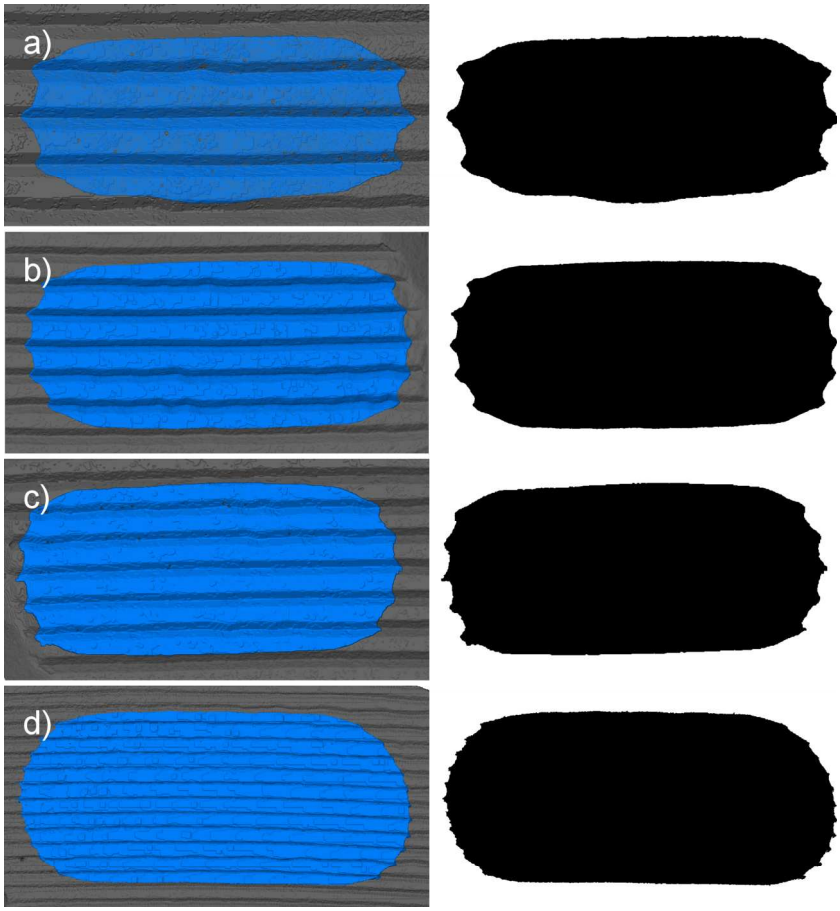

FIG. 10. Real wetted surface (left) and its projection on the reference plane (right) for drop 1 (a), drop 2 (b), drop 3 (c), and drop 4 (d).

holds for the cross-sectional slices: the contact line in each of them is similarly jagged, due to its pixelized nature, so its measurement is not straightforward. This issue is resolution-dependent, as the jagging obviously increases with the voxel dimension. Moreover, the presence of spurious steps in the extracted surfaces, e.g., caused by an imperfect planarity or alignment of the sample during the acquisition, may misleadingly increase the calculated real surface area. The size of this step corresponds exactly to the voxel size. In conclusion, the voxel size necessary for a correct roughness determination must be defined in relation with the smallest topology present in the anisotropic surface.

Such problem cannot even be solved by smoothing the extracted surfaces, as the gain in terms of reduction of spurious steps is counterbalanced by the reduction in the accuracy of tracking of the real contour. Figure 11 shows an example of the effects of different post-processing filters applied on drop 4, in order to evidence the cited issues.

Nevertheless, the problem of the measurement of feature contours is well-known and solutions having different complexities were discussed in the literature, particularly for 2D applications. For this work, the algorithm proposed in Ref. 22 was selected and applied on a slice basis. The contact line in each cross-sectional slice was expressed by means of a starting point and a chain code,[23] i.e., the steps necessary to walk from the starting point along all the pixels on that contour are memorized as numbers: 0 means "move right," 1 means "move diagonally to the upper right pixel," 2 means "move upwards," and so on. In this way, even values in the chain code indicate horizontal or vertical motion and odd values indicate diagonal motion. The number of changes between consecutive values in the chain code is also evaluated, metering the number of "corners" in the contour. The length of the real contour is then calculated as

$$L_{real} = 0.980 \cdot N_{even} + 1.406 \cdot N_{odd} + 0.091 \cdot N_{corner} \quad (1)$$

while the length L_{proj} of the projected contour is simply equal to the difference between the maximum and minimum horizontal coordinates of the contour. The real and projected

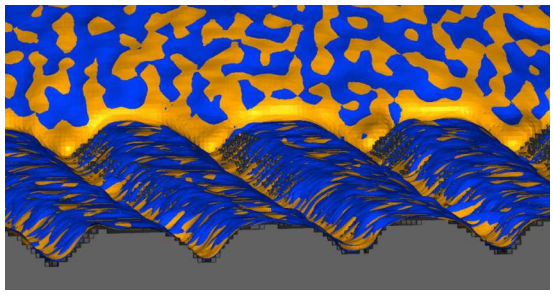

FIG. 11. Effect of filtering on contact surface appearance for drop 4. Figure shows a cross-section looked by inside: non-smoothed surface (grey) in which the raw voxelization is evident; smoothed surface by Gaussian filtering with 3 × 3 (blue) and 5 × 5 (yellow) voxel averaging.

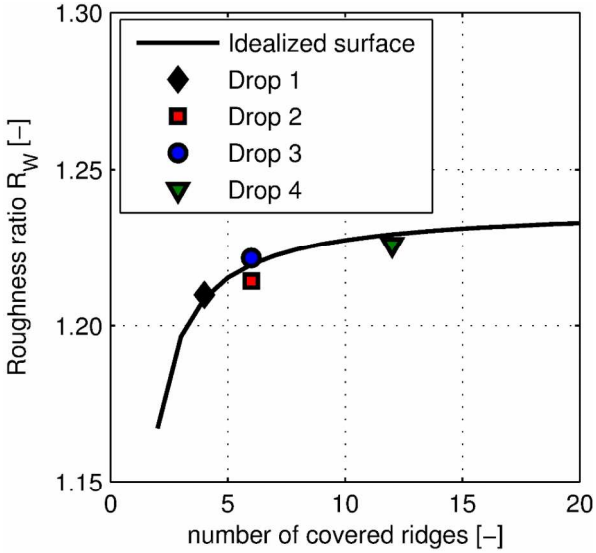

FIG. 12. Real wetted area ratio for complete wetting behavior.

contact line lengths are then summed up on all slices and the wetted area ratio is calculated assuming 1 voxel width for each line

$$R_W = \sum_i L_{real,i} \Big/ \sum_i L_{proj,i}. \quad (2)$$

Figure 12 reports the values of the roughness ratio R_W calculated with this approach, compared with the curve for the theoretical surface calculated using the geometrical values summarized in Table II. The calculated roughness ratios are in good agreement with the theoretical predictions. The values are, in general, slightly lower than the predictions with the theoretical calculation, which is correct as the latter does not take into account the fact that near its extremes the drops cover fewer ridges. The difference in R_W between drops 2 and 3 (having very similar volume and covering the same number of ridges) is linked to different wetting situations on the ridge edges as shown in Figures 10(b) and 10(c).

D. Partial wetting after surface treatment

The vinyl surface was also treated by TEGOTOP® 105 (Evonik Industries AG), a commercial concentrated dispersion

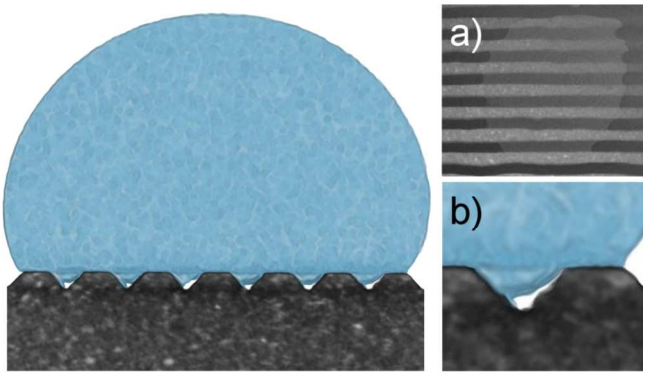

FIG. 13. Rendered tomographic acquisition of drop 5 deposed on the vinyl surface treated by a coating agent that shows hydrophobicity affected by disuniformity in the application.

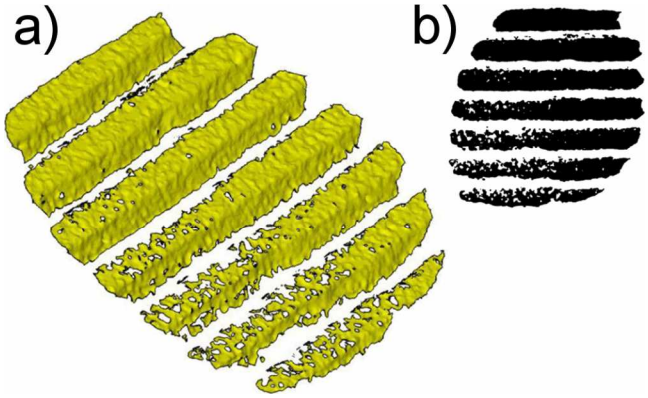

FIG. 14. Contact surface of drop 5 on the treated sample: (a) real wetted surface; (b) its projection on the reference plane.

of super-hydrophobic nano-agglomerates designed to equip a multitude of surfaces with the lotus effect *(Cassie-Baxter wetting regime)*. Figure 13(a) reports a rendered tomographic acquisition showing the wetting conditions after the treatment, while panel (b) evidences the effect of non-uniformity of application that causes only a partial hydrophobization.

Estimations of the real roughness ratio R_{CB} of the wetted surface in these conditions are impossible with any model or traditional technique, but it is achievable with microCT following the same approach described in Sec. III C. In this case, $R_{CB} = 1.145$. Figure 14 shows the real wetted surface and its projection on the reference plane.

IV. CONCLUSIONS

A novel technique for investigation of complete and partial anisotropic wetting on structured surface by X-ray microtomography is presented.

Three-dimensional equilibrium shapes of wetting drops deposited on an anisotropic surface, characterized by straight microfins of trapezoidal section, were investigated for the first time by micro computed tomography. Such technique allows to simultaneously digitize with micrometric spatial resolution the three-dimensional volume of a liquid–solid–gas system and its separating surfaces, with all the quantitative post-processing opportunities this may offer.

The novel technique (which is applicable to any structured surface) enables the direct measurement of the Wenzel roughness ratio based on the microCT scan in the wetted region. Comparison with idealized wetted surface is presented; congruence of results and effect of the scan resolution is evaluated and commented. An example of the wetted area ratio for partially wetting surface is also reported.

Regarding the comparisons with classical examples in Wenzel and Cassie-Baxter (partially hydrophobic) wetting regimes, the findings of the analyses on the tomographic volumes can be summarized as follows:

1. The preferential direction for drop contact line advancement is the one parallel to the grooves and it results in larger apparent contact angles on slices perpendicular to the groove direction. More in general, in regions where no

pinning on the edges of the surface is present, the real contact angle has the same value as on the flat surfaces; on the contrary where the triple line is pinned to the surface edges, much larger or much smaller apparent contact angles are measured.
2. If the drop and groove dimensions are comparable, the three-dimensional triple line of the equilibrium drop heavily depends on the surface pattern and simple geometrical contour shapes cannot be used as an equivalent contact line.
3. Extended filaments are formed within the grooves which feature a positive Laplace pressure.
4. The wetting state of the non-treated surface is of the Wenzel type, and the Wenzel roughness ratio increases with the number of ridges covered by the drop.

In summary, the presented technique proves to be very effective for both the qualitative and quantitative studies on complex surfaces.

ACKNOWLEDGMENTS

The financial support from the Regione Lombardia (Italy) within the call "Cooperazione Scientifica e Tecnologica Internazionale nelle aree tematiche agroalimentare, energia-ambiente, salute e manifatturiero avanzato" Project ID-MAN11, and the research fund grant to Maurizio Santini "Fondi di Ricerca di Ateneo," and even the prize "5 per 1000" of the University of Bergamo (Italy) are gratefully acknowledged. The research Grant of Stephanie Fest-Santini was financed within "Progetto ITALY®—Azione Giovani in Ricerca anno 2013" of the University of Bergamo (Italy). Professor G. Sotgia provided valuable advice. His contribution is gratefully acknowledged.

NOMENCLATURE

a	Drop minor axis (μm)
b	Drop major axis (μm)
Bo	Bond number (-)
g	Gravitational acceleration (m/s^2)
h	Groove height (μm)
L_{real}	Length of the real wetted surface (μm)
L_{proj}	Length of the projected wetted surface (μm)
p	Pitch (μm)
r	Radius (μm)
R_{CB}	Roughness ratio in Cassie-Baxter wetting regime (-)
R_W	Wenzel ratio (-)
V	Volume (mm^3)
w	Ridge width (μm)
σ	Surface tension (N/m)
ρ	Density (kg/m^3)

[1]P. de Gennes, F. Brochard-Wyart, and D. Quere, *Capillarity and Wetting Phenomena* (Springer, 2004).
[2]E. Bormashenko, *Wetting of Real Surfaces*, De Gruyter Studies in Mathematical Physics Vol. 19 (De Gruyter, Boston, 2013), see http://www.degruyter.com/view/product/129786.
[3]E. Bormashenko, Y. Bormashenko, G. Whyman, R. Pogreb, A. Musin, R. Jager, and Z. Barkay, "Contact angle hysteresis on polymer substrates established with various experimental techniques, its interpretation, and quantitative characterization," Langmuir **24**, 4020–4025 (2008).
[4]A. B. D. Cassie and S. Baxter, "Wettability of porous surfaces," Trans. Faraday Soc. **40**, 546–551 (1944).
[5]R. N. Wenzel, "Resistance of solid surfaces to wetting by water," Ind. Eng. Chem. **28**, 988–994 (1936).
[6]Y. Chen, B. He, J. Lee, and N. A. Patankar, "Anisotropy in the wetting of rough surfaces," J. Colloid Interface Sci. **281**, 458–464 (2005).
[7]J. Long, M. N. Hyder, R. Y. M. Huang, and P. Chen, "Thermodynamic modeling of contact angles on rough, heterogeneous surfaces," Adv. Colloid Interface Sci. **118**, 173–190 (2005).
[8]M. Morita, T. Koga, H. Otsuka, and A. Takahara, "Macroscopic-wetting anisotropy on the line-patterned surface of fluoroalkylsilane monolayers," Langmuir **21**(3), 911–918 (2005).
[9]M. Guilizzoni and G. Sotgia, "Experimental analysis on the shape and evaporation of water drops on high effusivity, microfinned surfaces," Exp. Therm. Fluid Sci. **34**, 93–103 (2010).
[10]H. Kusumaatmaja, R. J. Vrancken, C. W. M. Bastiaansen, and J. M. Yeomans, "Anisotropic drop morphologies on corrugated surfaces," Langmuir **24**, 7299–7308 (2008).
[11]M. Santini, M. Guilizzoni, and S. Fest-Santini, "X-ray computed microtomography for drop shape analysis and contact angle measurement," J. Colloid Interface Sci. **409**, 204–210 (2013).
[12]M. Santini and M. Guilizzoni, "3D X-ray micro computed tomography on multiphase drop interfaces: From biomimetic to functional applications," Colloids Interface Sci. Commun. **1**, 14–17 (2014).
[13]M. Mantegna and G. Sotgia, "Theoretical and experimental results about asymmetrical drops at rest upon surfaces having regular roughness," in *Proceedings of the ICHMT Meeting on Heat and Mass Transfer in Spray Systems, 05–10 June* (Antalya, Turkey, 2005).
[14]O. I. del Rio and A. W. Neumann, "Axisymmetric drop shape analysis: Computational methods for the measurement of interfacial properties from the shape and dimensions of pendant and sessile drops," J. Colloid Interface Sci. **196**(2), 136–147 (1997).
[15]R. E. Johnson and R. H. Dettre, "Contact angle hysteresis. III. Study of an idealized heterogeneous surface," J. Phys. Chem. **68**(7), 1744–1750 (1964).
[16]J. F. Oliver, C. Huh, and S. G. Mason, "Resistance to spreading of liquids by sharp edges," J. Colloid Interface Sci. **59**, 568–581 (1977).
[17]R. Shuttleworth and G. L. J. Baily, "The spreading of a liquid over a rough solid," Disc. Faraday Soc. **3**, 16–22 (1948).
[18]R. Seemann, M. Brinkmann, E. J. Kramer, F. F. Lange, and R. Lipowsky, "Wetting morphologies at microstructured surfaces," Proc. Natl. Acad. Sci. U.S.A. **102**(6), 1848–1852 (2005).
[19]A. D. Sommers and A. M. Jacobi, "Wetting phenomena on micro-grooved aluminum surfaces and modeling of the critical droplet size," J. Colloid Interface Sci. **328**, 402–411 (2008).
[20]F. Dutka, M. Napiórkowski, and S. Dietrich, "Mesoscopic analysis of Gibbs' criterion for sessile nanodroplets on trapezoidal substrates," J. Chem. Phys. **136**, 064702 (2012).
[21]D. C. Dyson, "Contact line stability at edges: Comments on Gibbs's inequalities," Phys. Fluids **31**, 229 (1988).
[22]A. M. Vossepoel and A. W. M. Smeulders, "Vector code probability and metrication error in the representation of straight lines of finite length," Comput. Graphics Image Process. **20**(4), 347–364 (1982).
[23]H. Freeman, "On the encoding of arbitrary geometric configurations," IEEE Trans. Electron. Comput. **EC-10**(2), 260-268 (1961).
[24]Just as a curiosity it is worth mentioning that the research of Sir G. N. Hounsfield (formerly employed at EMI Ltd., UK; Nobel Prize in 1979 with A. McLeod Cormack) for his part in developing the diagnostic technique of X-ray computed tomography was also supported by the large gains from The Beatles' vinyl music records like the used one.